International Information and
Engineering Technology Association
Advancing the World of Information and Engineering

Comparative Study of Fatigue Properties in Friction Stir Welded Dissimilar Aluminium Alloys (AA5083-H111 and AA6061-T6) Using an Optimized Tool Pin Profile Versus a Standard Design Tool

Wazir Hassan Khalafe[1]*, Ewe Lay Sheng[1], Muna Khethier Abbass[2], Mohd Rashdan Bin Isa[1], Shazarel Bin Shamsudin[3]

[1] Department of Mechanical Engineering, Universiti Tenaga Nasional, Kajang 43000, Malaysia
[2] Department of Production Engineering and Metallurgy, University of Technology, Baghdad 10066, Iraq
[3] Department of Manufacturing Engineering, Universiti Tun Hussein Onn Malaysia, Parit Raja 86400, Malaysia

Corresponding Author Email: wazirhassan495@yahoo.com

ABSTRACT

Friction stir welding (FSW) is a solid-state joining technique particularly effective for welding dissimilar aluminium alloys, such as AA5083-H111 and AA6061-T6. While the influence of FSW tool design on joint properties is acknowledged, the detailed comparative analysis of fatigue properties using different tool designs remains underexplored. This study fills this gap by examining the effects of a standard tool and an innovative tool design with longitudinal cylindrical grooves and circular grooves on the tool shoulder that are compatible with the thickness of the alloy to be welded. The tool designs were optimized using a systematic Design of Experiments (DOE) approach, focusing on enhancing mechanical properties and fatigue life through controlled tool features and process parameters. The tensile strength of the welded joints was quantitatively assessed, revealing that joints produced with the novel tool (S1) achieved a significantly higher tensile strength of 317 MPa (±15 MPa), compared to 285 MPa (±13 MPa) for the standard tool (S2). This improvement is linked to the novel tool's optimized heat generation and material flow characteristics. Moreover, the microstructure and hardness across the weld zones were evaluated to further understand the impact of tool design on the welding outcomes. Fatigue tests were conducted on samples from both tool types at seven different stress levels. The fatigue life, represented through S-N curves, showed that at an applied stress of 160 MPa, specimens welded with the novel tool withstood up to 9,328,980 cycles before failure, surpassing the 7,589,146 cycles endured by the standard tool, indicative of superior fatigue resistance. These results highlight the critical role of tool design in enhancing the FSW process for dissimilar aluminium alloys, demonstrating both the scientific rigor and innovative scope of the study.

1. INTRODUCTION

Friction stir welding (FSW) is renowned for its superior mechanical properties and minimal defects, making it a preferred method for engineering applications, especially in welding aluminum alloys like 5083-H32 and 6061-T6 [1, 2]. Since its inception in 1991, FSW has offered significant environmental benefits and cost-effectiveness compared to traditional welding methods, leading to its widespread adoption [3]. The technique has undergone extensive development over the years, particularly enhancing its fatigue performance, an essential factor for modern manufacturing processes.

Studies by Abbass et al. [4] and Mousa et al. [5] have shown that FSW achieves high joint efficiency with controlled rotational speeds and feed rates. However, these studies have primarily focused on similar alloys, leaving a notable gap in our understanding of how different alloy behaviors, such as those between AA5083-H111 and AA6061-T6, influence

weld quality under analogous conditions. Further researches by Zhang et al. [6] and Wang et al. [7] had illuminated how microstructural features like notch locations and cooling methods can impact the fatigue life of welded joints. Nevertheless, there is a lack of comprehensive exploration into the specific effects of innovative tool designs on these properties in dissimilar alloys. Mahenran and Rajammal [8] used ultrasonic stir casting method, and the hybrid aluminium nano composite material was successfully fabricated.

Lu et al. [9] contributed to this area by introducing a lifecycle prediction model that incorporates damage defects as a variable, thus enhancing our grasp of the lifecycle impacts under varied FSW conditions. Still, the potential for exploring how tool design affects these dynamics remains largely untapped. Similarly, works by Chen et al. [10] and Kumar et al. [11] had documented that FSW induces heterogeneous microstructures that significantly influence the mechanical properties and fatigue responses of the welds, yet the relationship between tool design, microstructural

heterogeneity and mechanical properties in dissimilar aluminum alloy welds has not been thoroughly investigated.

Salim et al. [12] found repairing structures damaged by fatigue through the use of composite patch bonding is an efficient and economical process to preserve structures and increase their lifespan

This study seeks to bridge these identified gaps by investigating the effects of innovative tool designs on the fatigue properties and mechanical integrity of friction stir welded dissimilar aluminum alloys (AA5083-H111 and AA6061-T6). FSW has been noted for its enhanced fatigue resistance in aluminum and magnesium alloys compared to traditional fusion welding methods [13]. A comparative study has shown that FSW weld metal exhibits the lowest fatigue crack growth rate, while gas tungsten arc welding (GTAW) records the highest, with base metal samples displaying intermediate rates [14]. By employing both standard and novel tool designs, this research aims to measure maximum tensile strength and analyze fracture surfaces using Scanning Electron Microscopy (SEM), providing new insights into optimizing FSW for superior industrial applications.

2. EXPERIMENTAL PROCEDURE

This section details the preparation and analysis of samples for friction stir welded materials, emphasizing a systematic and optimized approach. The process begins with selecting suitable materials, preparing the plates, and carefully designing the welding tools. Specific welding parameters are precisely calibrated based on the Design of Experiments (DOE) methodology, which ensures statistical reliability and a structured experimental framework.

To optimize the friction stir welding (FSW) process, this study employs Response Surface Methodology (RSM) within the DOE framework. This approach effectively reduces the number of experimental trials while identifying optimal conditions to maximize ultimate tensile strength (UTS). By facilitating rigorous hypothesis testing, DOE enables controlled experiments that systematically assess the effects of various welding parameters on material properties. The experimental setup includes a half-factorial design with two replicates and three central points, as shown in Table 1, focusing on key factors such as material thickness, tool rotational speed, holding time, tool pin length and feed rate. These parameters are varied as follows: material thickness from 3 to 5 mm, holding times from 15 to 25 seconds, tool pin lengths from 0.1 to 0.3 mm, rotational speeds from 800 to 1600 RPM, and feed rates from 30 to 90 mm/min (detailed in Table 2). UTS is selected as the primary response variable for analysis. Moreover, a 32 full factorial design is employed to investigate the effects of stationary welding forces on process parameters. This design involves 12 experimental runs, including a central point replicated four times to mitigate variability. This comprehensive experimental strategy, combining DOE and RSM, ensures reliable findings while efficiently optimizing welding parameters to enhance mechanical performance. It highlights the integration of statistical rigor and engineering precision to achieve superior material properties.

In this study, 19 samples were prepared for each tool design to collect comprehensive data. However, for microhardness and fatigue life tests, only the samples exhibiting the highest tensile strength (TS) from each tool design, the standard (S2)

and the innovative designed tools (S1), were selected. This selective focus ensures an evaluation of peak performance characteristics under optimal conditions, providing insights into the correlation between tensile properties and durability under cyclic stress.

Table 1. Experimental design using ½ factorial design

Run Order	Input Parameters (Factors)				
	Th	Tt	L	SS	Fr
1	3	25	0.3	1600	90
2	3	15	0.3	800	90
3	5	25	0.1	1600	90
4	4	20	0.2	1200	60
5	3	25	0.1	1600	30
6	5	15	0.3	1600	90
7	3	25	0.1	800	90
8	5	25	0.3	1600	30
9	4	20	0.2	1200	60
10	3	15	0.1	1600	90
11	4	20	0.2	1200	60
12	5	15	0.1	1600	30
13	3	15	0.1	800	30
14	3	15	0.3	1600	30
15	3	25	0.3	800	30
16	5	25	0.3	800	90
17	5	15	0.3	800	30
18	5	25	0.1	800	30
19	5	15	0.1	800	90

Table 2. Design of the process parameters

Factor Symbol	Parameter	Level		
		Low (−1)	Center (0)	High (+1)
Th	Thickness (mm)	3	4	5
Tt	Holding time (s)	15	20	25
L	Length (mm)	0.1	0.2	0.3
SS	Spindle speed (RPM)	800	1200	1600
Fr	Feed rate (mm/min)	30	60	90

2.1 Samples preparation

2.1.1 Materials and preparation for welding

The preparation phase involves cutting aluminum alloys AA6061-T6 and AA5083-H111 into samples of varying thicknesses (3, 4, and 5 mm) using a precision laser cutting machine. These dimensions ensure uniformity and precision in the testing process. The FSW process employs both a standard tool and a newly developed tool design, tailored for this research, to perform welding under controlled parameters such as alloy thickness, tool traverse speed, stirrer length, stirrer speed and feed rate.

2.1.2 Preparation of plates and tool design for welding

Both standard and innovative tool designs are crafted from high carbon steel. The innovative tool design features a cylindrical pin with longitudinal grooves and a variable length, engineered to optimize heat generation and material flow during welding as shown in Figure 1. The adjustable pin length and grooved shape allow for tailoring mechanical properties to different material types and thicknesses, extending the tool's lifespan and minimizing wear [15]. The shoulder diameter is calculated using the formula:

$$D = (d \times 3) + 2 \, mm,$$

where, d is the thickness of the metal as shown in Table 3.

(a)   (b)
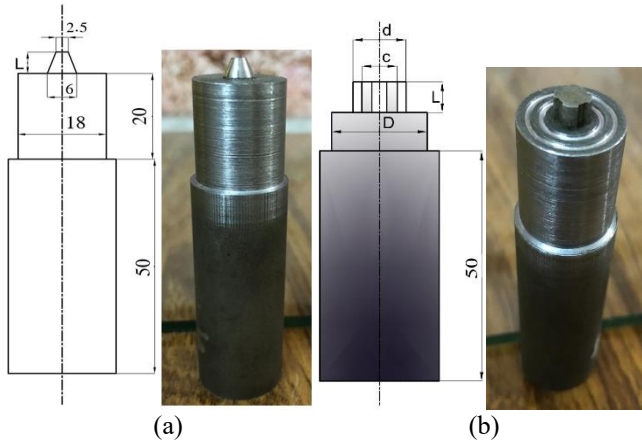
Figure 1. (a) Normal tool design (b) New tool design

Table 3. New tool parameters

	Details	Dimension
L	Length of tool pin (mm)	d - (0.1,0.2,0.3) mm, less than the material thickness for FSW welding
d	Diameter of tool pin (mm)	material thickness to be welded
C	d - 1 mm, where 1 mm, Depth digging groove × 2	Depth digging in surface of shoulder= 0.5 mm
D	Diameter of shoulder (mm)	(d*3) + 2 mm
	Pin profile: Cylindrical with groove	
	Title angle (1.60)	
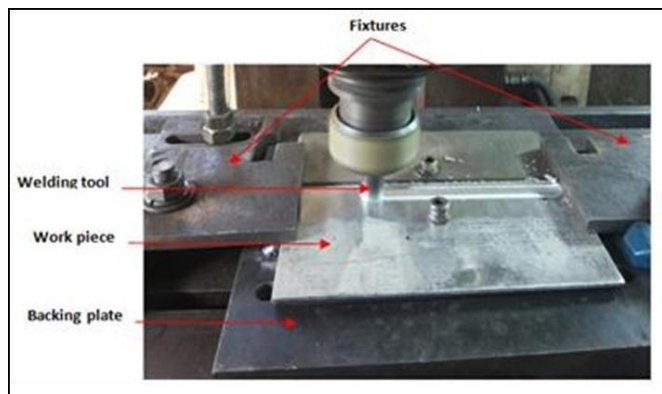
Figure 2. The machine of friction stir welding

The symmetrical circular grooves on the shoulder, each 0.5 mm deep, are crucial for maintaining uniform material mixing and plastic deformation. This design is expected to enhance plastic deformation, leading to a more consistent and high-quality weld seam. The pin's unique geometry is specifically tailored to improve the mixing of materials, crucial for achieving superior mechanical properties across different material types and thicknesses. Conversely, the standard tool design consists of a simpler pin shape, which does not facilitate as dynamic a material flow or heat generation. The standard tool design, as shown in Figure 1(a), consists of a pin

that is 0.1, 0.2, or 0.3 mm shorter than the metal thickness, tapering from a 2.5 mm diameter at the end to 6 mm at the shoulder. The shoulder has a diameter of 18 mm and the overall tool length is 50 mm, suitable for mounting on the FSW machine. Before welding, the samples are securely fixed using a fixture and backing plate attached to the base of the milling machine, as depicted in Figure 2.

2.1.3 Welding process parameters

The welding process parameters such as linear speed, tool rotational speed and tool tilt angle are meticulously controlled. Each parameter plays a crucial role in influencing the weld's mechanical, metallurgical and microstructural properties. The settings for these parameters were determined through the DOE, ensuring each adjustment contributes optimally to the desired outcomes. For example, the tool tilt angle affects the depth of penetration and the width of the heat-affected zone, which in turn influences the tensile strength and fatigue life of the weld.

The FSW process involves four key stages: plunging, penetration, stirring and completion. During welding, the joint is characterized by two distinct sides: the advancing side, where the linear and rotational speeds move in the same direction and the retreating side, where they move in opposite directions [16].

2.2 Samples characterization

2.2.1 Microstructure and hardness tests

Microstructure analysis and Vickers micro-hardness tests are conducted to evaluate changes in the weld's microstructure across various zones: stir zone (SZ), thermo-mechanical affected zone (TMAZ), heat-affected zone (HAZ) and base metal (BM). These tests are crucial for understanding how the weld's characteristics vary across different regions and under different tool designs.

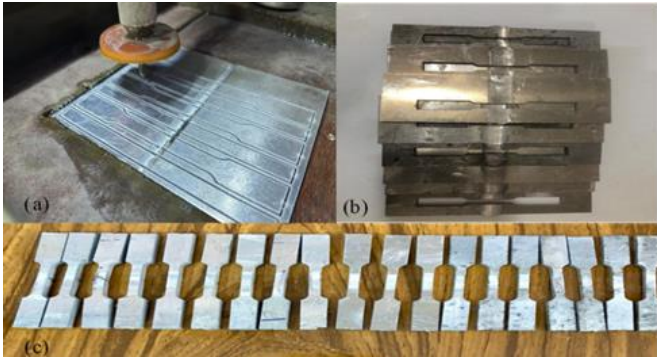2.2.2 Tensile test

Tensile tests are performed by tensile strength machine (Figure 3) to determine the ultimate tensile strength of the samples, adhering to ASTM E8/E8M-15a standards. This testing is crucial for assessing the mechanical strength of the welds. Figure 4 depicts the precision cutting of the samples using a CNC water jet for subsequent analysis.

**Figure 3.** Tensile strength machine

Figure 4. Welded samples preparation for TS test: (a) CNC jet water; (b) Cutting samples for tensile tests; (c) Tensile strength samples (E8/E8M 15a)

2.2.3 Fatigue life test

The fatigue testing was carried out with a SHIMADZU EHF-020-OA machine, designed to apply different stress levels under room temperature conditions and without any mean stress. Fatigue testing assesses the durability of the welds under cyclic loading, crucial for applications where the material must withstand repeated stress. This testing helps plot the S-N curve, which is vital for understanding the fatigue life of the materials used (Figure 5).
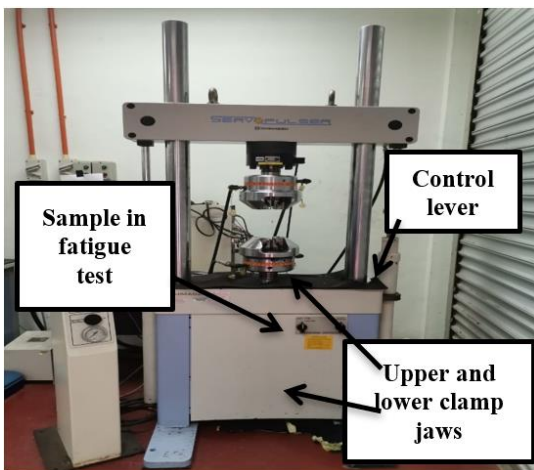
Figure 5. Fatigue dynamic testing machine - Shimadzu Servo pulser EHF Machine

3. RESULTS AND DISCUSSION

3.1 Tensile test results

This study focuses on optimizing friction stir welding (FSW) parameters using an innovative tool design (S1) in comparison with a standard design (S2), employing the ANOVA method. Key variables include Thickness (Th: 3-5 mm), Holding Time (Tt: 15-25 seconds), Length (L: 0.1-0.3 mm), Spindle Speed (SS: 800-1600 RPM), and Feed Rate (Fr: 30-90 mm/min).

In tensile strength comparisons, sample S1, using AA6061 and AA5083 materials, achieved a maximum ultimate tensile strength (UTS) of 317 MPa under specific settings: Thickness of 3 mm, Holding Time of 25 seconds, Length of 0.1 mm, Spindle Speed of 1600 RPM and Feed Rate of 30 mm/min. In contrast, sample S2 recorded a maximum UTS of 285 MPa with parameters including a 5 mm Thickness, 25-second

Holding Time, Length of 0.3 mm, Spindle Speed of 800 RPM, and Feed Rate of 90 mm/min. The FSW joint efficiency was also evaluated, revealing a significant improvement with the innovative tool design. Joints produced with the standard tool achieved an efficiency of 83%, while those made using the new tool design reached a superior efficiency of 92.2%. FSW relies on a rotating tool to generate heat through friction, softening the material and enabling it to mix and bond as it cools. Variations in tool design influence weld efficiency and strength by altering heat generation and material flow during the process. These results highlight the effectiveness of this innovative tool design in producing stronger and more efficient welded joints.

19 samples were analyzed to evaluate tensile strength, and the findings, summarized in Table 4, highlight the significantly higher tensile strength achieved with the innovative tool. The study validated the mechanical performance of aluminium alloy specimens (AA6061-T6 with AA5083-H111) welded using the novel tool, with a UTS of 317 MPa corresponding to a weld joint efficiency of 93%. This represents a substantial improvement over previously reported results.

On the other hand, for standard tool design, the highest recorded ultimate tensile strength (UTS) of 285 MPa was achieved under the following specific conditions: 3 mm sheet thickness, 25-second holding time, 0.3 mm tool pin length, 800 RPM spindle speed, and a feed rate of 90 mm/min (Table 5). These results show the critical influence of holding time, feed rate and rotational speed on UTS, while spindle speed and sheet thickness exerted comparatively less pronounced effects on the welding process. Notably, the standard tool design achieved higher UTS at 800 RPM and a welding rate of 90 mm/min, likely due to the substantial frictional heat generated under these conditions, enhancing material bonding and weld strength.

3.2 Microstructure results

The microstructure of the welded samples (S1 and S2), producing the highest tensile strength, is illustrated in Figures 6 and 7, showcasing the joint between two similar aluminum alloys (AA5083-H111 and AA6061-T6). Figure 6 highlights the complex microstructure across various zones of a friction stir welded joint using a new tool design. Central to our analysis is the stir zone (SZ) or nugget zone, located at the weld's center, where complete recrystallization occurs, indicating a transformation due to the welding process. This zone, significantly influenced by the new tool, features grains dramatically smaller than those in untreated materials, signifying a thorough blending of the dissimilar alloys. Grain refinement occurs due to the high-strain deformation and thermal cycles, as supported by recrystallization theories. Adjacent to the SZ is the Thermo-Mechanically Affected Zone (TMAZ), depicted in Figures 6 (a) and (b), where the material undergoes substantial but not complete recrystallization due to the combined thermal and mechanical forces during welding. The Heat Affected Zone (HAZ), shown in Figures 6 (a), (c) and 5 (b), experiences thermal modifications from the welding but lacks notable plastic deformation. It displays a microstructure similar to the base materials, with minimal changes. At the outermost parts of the cross-section are the Base Material (BM) regions (Figures 6(b) and (f)), which remain essentially unaltered, marking the original state of the AA5083 and AA6061 alloys. Contrasting this, the use of a

standard tool design results in larger grain sizes within the SZ, as shown in Figure 7, correlating with reduced mechanical properties, a tensile strength of 285 MPa and a hardness of 101 HV (Figure 8). This comparison highlights the significant role of tool design in influencing the microstructure and thereby the mechanical characteristics and durability of the weld. The new tool design optimizes material mixing and heat generation, leading to a superior microstructural formation and enhanced joint properties. These observations align with existing research [17], further validating our understanding of the friction stir welding process and its intricate dynamics.

TS of friction stir welding (FSW) using a new tool design (S1) at the welded joint. (a) The left-side base metal (BM), AA5083, is on the advancing side. (b) Next to the advancing side is the Thermo-Mechanically Affected Zone (TMAZ). (c) The Heat Affected Zone (HAZ) is found beyond the TMAZ. (d) The center of the joint features the Stir Zone (SZ), also referred to as the nugget zone. (e) A TMAZ is present on the retreating side. (f) The right-side BM, consisting of AA6061-T6, is situated on the retreating side.

Table 4. Tensile strength from using new design tool of FSW

| No. | Input Parameters (Factors) | | | | | Response | | |
	Thickness (mm)	Time holding (second)	Length (mm)	Rotation tool speed r.p.m	Linear tool speed mm/min	Yield stress (MPa)	Elongation %	Average (MPa) used Innovative design tool
1	3	25	0.3	1600	90	255	0.512	285
2	3	15	0.3	800	90	240	8.335	280
3	5	25	0.1	1600	90	210	7.82	250
4	4	20	0.2	1200	60	210	0.817	245
5	3	25	0.1	1600	30	300	2.249	317
6	5	15	0.3	1600	90	195	0.92	197
7	3	25	0.1	800	90	270	1.14	290
8	5	25	0.3	1600	30	210	0.861	270
9	4	20	0.2	1200	60	230	0.531	240
10	3	15	0.1	1600	90	134	0.561	205
11	4	20	0.2	1200	60	140	0.878	245
12	5	15	0.1	1600	30	168	0.555	215
13	3	15	0.1	800	30	140	0.262	153
14	3	15	0.3	1600	30	142	0.923	220
15	3	25	0.3	800	30	215	8.65	250
16	5	25	0.3	800	90	230	1.07	285
17	5	15	0.3	800	30	194	1.037	196
18	5	25	0.1	800	30	270	9.301	278
19	5	15	0.1	800	90	66	0.703	190

Table 5. Tensile strength results obtained using standard tool design

| Run Order | Input Parameters (Factors) | | | | | Response | |
	Th	Tt	L	SS	Fr	Average Measured Value (TS)	% Error
1	3	25	0.3	1600	90	282	0.89
2	3	15	0.3	800	90	209	0.67
3	5	25	0.1	1600	90	211	0.80
4	4	20	0.2	1200	60	209	0.72
5	3	25	0.1	1600	30	282	0.57
6	5	15	0.3	1600	90	146	0.66
7	3	25	0.1	800	90	282	0.88
8	5	25	0.3	1600	30	227	0.68
9	4	20	0.2	1200	60	195	0.65
10	3	15	0.1	1600	90	155	0.78
11	4	20	0.2	1200	60	209	0.90
12	5	15	0.1	1600	30	155	1.23
13	3	15	0.1	800	30	146	0.94
14	3	15	0.3	1600	30	195	1.36
15	3	25	0.3	800	30	227	0.89
16	5	25	0.3	800	90	285	0.96
17	5	15	0.3	800	30	146	1.15
18	5	25	0.1	800	30	237	0.98
19	5	15	0.1	800	90	164	0.75
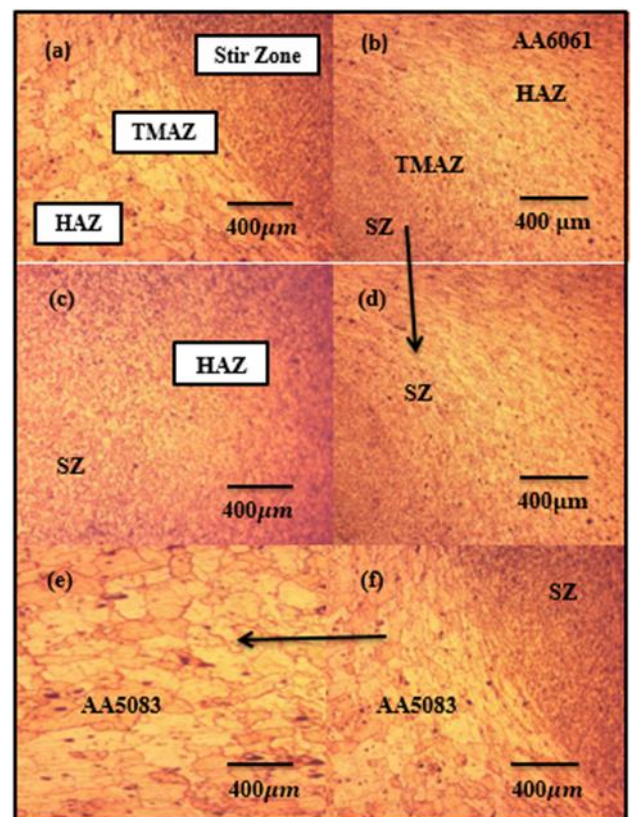
Figure 6. The microstructure of the optimal tool shoulder
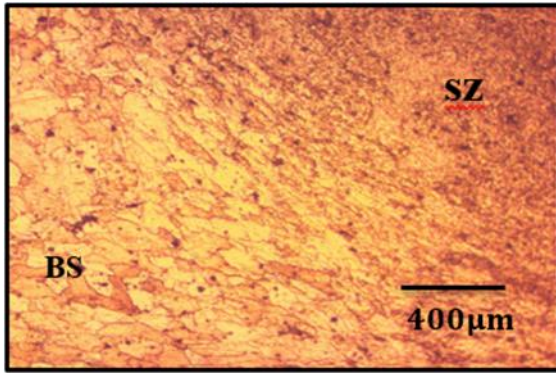
Figure 7. The microstructure within the side of the welded joint. The optimal tensile strength's microstructure for friction stirs welding using standard tool design (S2)
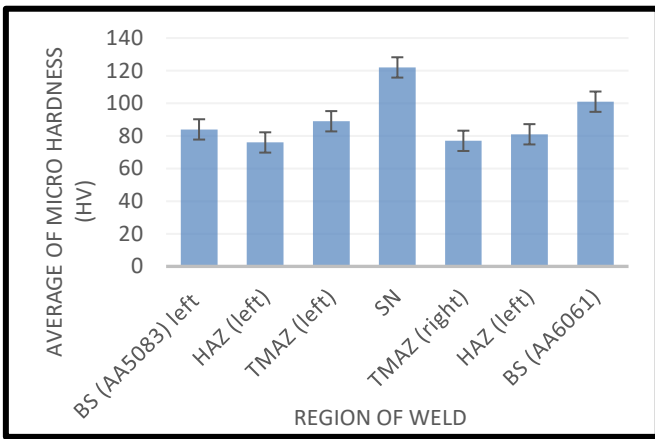
Note: Base Metal (BM), Heat Affected Zone (HAZ), Thermo-Mechanically Affected Zone (TMAZ). Error bars are for 95% confidence intervals.

Figure 8. Average of microhardness (HV) in region of weld sample 3

3.3 Micro hardness results

Table 6 summarizes the microhardness results obtained under conditions optimized for tensile strength (TS) using the innovative designed tool. The microhardness values, measured in the stir zone (SZ) using Vickers microhardness (HV), range from 105 to 122. These variations, alongside the optimal tensile strengths, highlight the intricate nature of the Friction Stir Welding (FSW) process, where multiple interacting factors influence the final outcomes.

Table 6. Microhardness of optimum TS of FSW with innovative tool design

No. of Samples	Optimize TS	Micro Hardness (Average SZ)	Error Margins
	MPa	HV	
1	285	120	15
2	280	118	11
5	317	122	17
7	290	105	20
8	270	105	25
18	278	105	20

Detail of samples data as follow:
- Sample 1: TS 285 MPa (Th 3 mm, Tt 25 s, L 0.3 mm, SS 1600 rpm, Fr 90 mm/min);
- Sample 2: TS 280 MPa (Th 3 mm, Tt 15 s, L 0.3 mm, SS

800 rpm, Fr 90 mm/min);
- Sample 5: TS 317 MPa (Th 3 mm, Tt 25 s, L 0.1 mm, SS 1600 rpm, Fr 30 mm/min);
- Sample 7: TS 290 MPa (Th 3 mm, Tt 25 s, L 0.1 mm, SS 800 rpm, Fr 90 mm/min);
- Sample 8: TS 270 MPa (Th 5 mm, Tt 25 s, L 0.3 mm, SS 1600 rpm, Fr 30 mm/min);
- Sample 18: TS 278 MPa (Th 5 mm, Tt 25 s, L 0.1 mm, SS 800 rpm, Fr 30 mm/min).

A notable observation is the apparent correlation between tensile strength and microhardness. For example, the sample achieving the highest TS of 317 MPa also recorded the highest microhardness value of 122 HV. This relationship likely stems from the intrinsic mechanisms of the FSW process, wherein higher tensile strengths may be associated with denser, refined grain structures, contributing to enhanced microhardness.
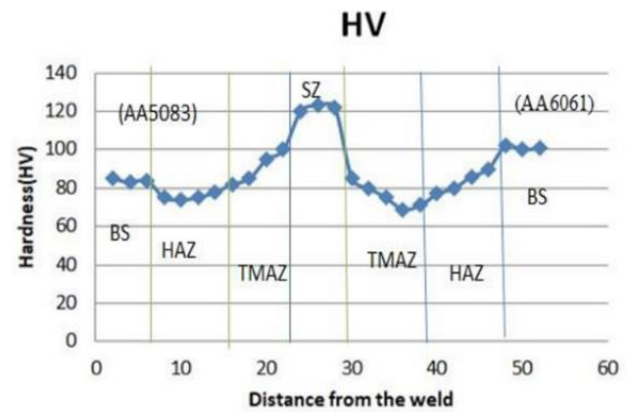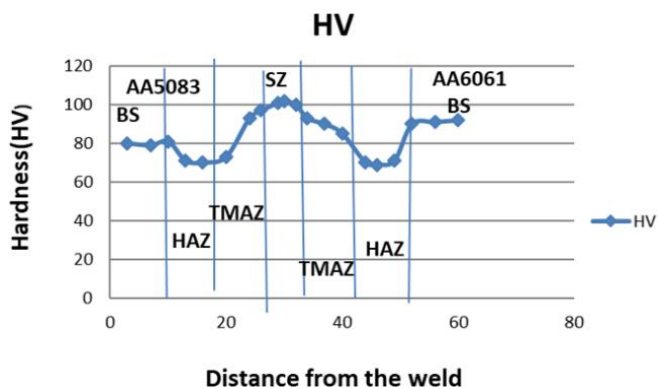

Figure 9. Micro-hardness distribution across the AA5083-H111 and AA6061-T6 weld cross-section, using optimal conditions and innovative tool design (S1), showed a maximum tensile strength of 317 MPa

The sample displaying the highest tensile strength (TS) of 317 MPa (S1) also presents a notable micro-hardness value of 122 HV in the stir zone (SZ), illustrating the significant correlation between TS and micro-hardness due to the welding process. Such correlation suggests that higher TS may be linked to denser grain structures within the SZ, as seen in Figure 9 which showcases the varying hardness values across different weld zones. In detail, the friction stir welding analysis, using a new tool design, reveals distinct differences in hardness across four critical zones of the weld. The base metal (BM) consists of original materials AA5083 and AA6061, serving as the foundational elements of the weld. The Thermo-Mechanically Affected Zone (TMAZ) and the Heat-Affected Zone (HAZ) around the weld are influenced by thermal and mechanical stress, altering their hardness properties. The SZ, where the actual mixing of metals occurs, is crucial as it directly affects the weld's strength and quality. The SZ demonstrates a significantly higher average hardness (122 HV) compared to the HAZ, attributed to recrystallization processes that lead to refined, equiaxed grain structures. While the HAZ shows a decrease in hardness, the TMAZ exhibits a slight increase, indicating robust microstructure recovery due to the fine grain structure. Previous studies [18, 19] have noted similar patterns, but our findings with the new tool design show enhanced hardness levels, suggesting improvements in the tool's efficiency and effectiveness. Reference [20], details a study where friction stir welding was performed on AA6061

aluminum with a thickness of 6 mm using a standard tool. The experiment varied tool rotational speeds (1400, 1200, and 1000 rpm), bed speeds (30, 25, and 20 mm/min) and axial loads (7, 6, and 5 kN). The resulting hardness values averaged at 85, 77, and 87 HV. Comparatively, our new tool design achieves higher hardness, suggesting it improves the welding process, possibly through better heat management and material flow, leading to enhanced grain refinement and stronger joints. Another research by Manuel et al. [21], on three dissimilar aluminum alloys welded in a T-joint configuration under varied conditions further supports our observations, indicating that FSW with innovative tool designs can significantly influence material properties through refined grain structures, optimizing mechanical properties in welded joints.

Figure 10 illustrates the micro-hardness distribution across the weld cross-section of AA5083-H111 and AA6061-T6 alloys under optimal welding conditions using a standard tool. The analysis highlights the hardness values within the weld region and its surrounding areas, focusing particularly on this optimal sample. In the analyzed sections, the stir zone (SZ) demonstrated the highest average hardness, recorded at 101 HV. This peak hardness in the SZ is attributed to the dynamic recrystallization and grain refinement processes that occur during welding. Micro-hardness testing across various points of the weld region—specifically the SZ, thermo-mechanically affected zone (TMAZ), heat-affected zone (HAZ) and base metal (BM). It helps to elucidate the changes in microstructure, confirming that the SZ exhibits greater hardness compared to the TMAZ, HAZ and unaffected areas.

Figure 10. Micro-hardness distribution across the AA5083-H111 and AA6061-T6 weld cross-section, using optimal conditions and a standard design tool (S2), showed a maximum tensile strength of 285 MPa

Materials exhibit diverse mechanical behaviors, with tensile strength (TS) reflecting resistance to pulling forces and microhardness (HV) indicating resistance to localized deformation (Figure 8). Although both metrics provide insights into a material's mechanical strength, they do not always correlate due to differences in testing methodologies, material microstructures and processing influences. Tensile tests evaluate a material's ability to withstand elongation under stress, whereas hardness tests focus on localized resistance to compressive forces. In addition, the arrangement of atoms or grains within the material can affect tensile strength and hardness differently. Consequently, processing parameters that enhance one property may not necessarily improve the other, emphasizing the importance of understanding these distinct influencing factors for accurate

and effective material customization.

This research demonstrates that friction stir welding (FSW) produces weld joints with superior tensile properties and impact strength compared to the parent material. This improvement is attributed to the fine microstructure and increased hardness achieved during the process. FSW generates heat through the friction of a non-consumable rotating tool against the substrate and the deformation caused by the tool traversing the material. The heat generated leads to volumetric heating, enabling the creation of a continuous solid-state joint as the tool progresses. Unlike fusion welding, FSW avoids solidification-related defects, making it a reliable method for producing high-quality joints.

The process typically involves arranging the materials to be joined in a butt configuration, where the rotating tool is brought into contact with the workpieces. The tool consists of two main components: the probe, which protrudes from the tool's lower surface, and the shoulder, which has a larger diameter. Tool design is critical in FSW, as optimized geometry can enhance heat generation and stirring efficiency, leading to faster welding speeds and higher-quality welds. The materials used for the tool must possess high hardness at elevated temperatures and maintain this hardness over extended periods to ensure durability. The combination of tool material and base material plays a crucial role in the tool's lifespan and overall performance.

During welding, the workpieces are securely clamped onto a backing bar to prevent joint faces from separating or misaligning. The friction between the wear-resistant tool and the workpieces generates sufficient heat to soften the materials without melting them. As the tool moves along the weld line, the softened material flows from the leading edge of the tool to the trailing edge, where it is forged together under the pressure of the tool shoulder and pin. This creates a solid-phase bond with a refined microstructure.

FSW is a continuously evolving technology in the field of metal joining, with the quality of welds heavily influenced by the appropriate selection of the welding tool. The pin profile, shoulder design, and tool material significantly affect the uniformity of the microstructure and the mechanical properties of the weld. Tools must be strong enough to endure high temperatures and facilitate effective material mixing in the weld zone. Studies on the influence of tool geometry reveal that different tool shapes result in variations in weld hardness and tensile strength, highlighting the importance of tool design in controlling material flow and achieving consistent weld quality.

According to Hall-Petch theory, a finer and smaller average grain size significantly enhances microhardness when using the innovative designed tool. The results indicate that grain size reduction plays a crucial role in the consistent improvement of microhardness. Furthermore, the profiles exhibit smaller chip boundaries and grain sizes, with minimal voids and fewer cracks, contributing to the superior mechanical properties observed.

3.4 Fatigue test results

The design of the friction stir welding (FSW) tool plays a pivotal role in ensuring the effectiveness of the welding process, particularly in generating the heat necessary to achieve optimal mechanical properties in the weld zone. However, tool longevity remains a critical challenge, especially when welding materials with high melting points,

which limits FSW's broader industrial applicability. Continuous research into tool design has refined features such as the shoulder and pin, leading to improved material flow, enhanced mixing and reduced process loads.

Both the standard and innovative tool designs, crafted from high-carbon steel, underscore the significance of geometry optimization in the FSW process. The newly designed tool introduces several advanced features that enhance the welding process. Longitudinal grooves on the cylindrical pin significantly improve heat generation, which is crucial for effective plastic deformation and high-quality welds. These grooves also facilitate improved material flow and mixing, resulting in a more uniform weld seam. Also, symmetrical circular grooves, 0.5 mm deep, on the tool shoulder contribute to consistent material mixing and deformation. The innovative design also incorporates a dynamically adjustable pin length, enabling the customization of mechanical properties to optimize weld quality and efficiency. This versatility allows the tool to accommodate various material types and thicknesses, extending its lifespan while reducing wear. Despite these advancements, some limitations of the FSW process remain. These include the exit hole left upon tool withdrawal, the need for significant downward force and heavy-duty clamping to secure the plates, limited flexibility with thickness variations and non-linear welds and a slower traverse rate compared to certain fusion welding techniques. However, the slower rate can often be offset by the reduction in the number of welding passes required.

This section focuses on the discussion of fatigue test results. Fatigue testing at seven different stress levels (measured in MPa) was conducted on the welded joints of samples S1 and S2 (Table 7). This testing aimed to evaluate the durability of joints produced with two different tool designs. This differentiation in tool designs emphasizes the innovative approach taken in this study. All samples adhered to ASTM E466-15 standards and were tested under a stress ratio of R=-1 to evaluate their fatigue life.

Table 7. Results of stress amplitude and number of cycles for FSW (AA5053-H111 with AA6061-T6) Standard design tool and FSW (AA5053-H111 with AA6061-T6) Innovative design tool

FSW (AA5053-H111 with AA6061-T6) Standard Design Tool (S2)		FSW (AA5053-H111 with AA6061-T6) New Design Tool (S1)	
Stress (MPa) σ	Cycle, N	Stress (MPa) σ	Cycle, N
260	269274	260	532983
220	341646	220	724709
200	639699	200	1299227
190	1463509	90	1950290
180	2400059	180	3065673
170	4078785	170	5038965
160	7589146	160	9328980

The results, illustrated in Figure 11, highlight the superior fatigue resistance conferred by the new tool design. Under an applied stress of 160 MPa, S1 endured 9,328,980 cycles before failure, significantly outperforming the 7,589,146 cycles achieved by S2. This enhanced performance is attributed to the new tool's advanced heat management during the welding process, which not only improved mechanical and metallurgical properties but also induced beneficial residual stresses, plastic strains, and enhanced weld homogeneity. This pioneering tool design thus significantly increases the fatigue

strength of the welds, demonstrating a clear technological advancement in friction stir welding. This study's findings offer compelling evidence of the benefits of innovative tool design in enhancing the durability and reliability of welded joints across all applied loads.
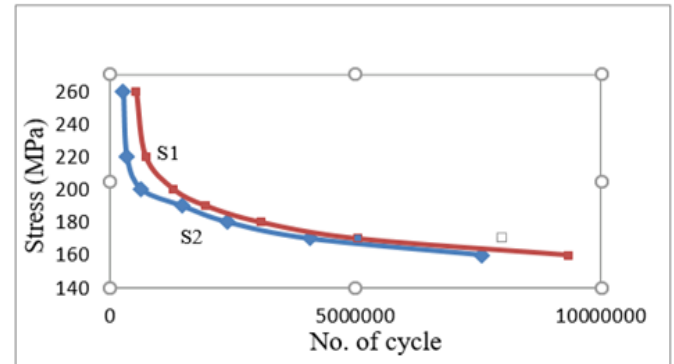
Figure 11. Fatigue behavior of FSW used standard design tool (S2) and FSW used new design tool (S1)

3.5 Fractography results

The fractography of welded sample S1, illustrated in Figure 12, provides an in-depth analysis of the fracture surfaces, revealing distinct morphological features that elucidate the fracture mechanisms. An initial examination at 25x magnification (Figure 12(a)) displays the overall morphology and roughness of the fracture surface, setting the stage for a detailed investigation of material behavior during welding. At 50x magnification, Figure 12(b) highlights a textured surface adorned with visible microvoids, indicative of the material's plastic deformation under stress. Further examination at 75x magnification in Figure 12(c) reveals conical, equiaxed dimples, a characteristic of ductile fracture in aluminum alloys, suggesting significant energy absorption before failure. The most detailed examination at 100x magnification (Figure 12(d)) shows shallow and small dimples, confirming the ductile nature of the fracture and the material's capacity for extensive plastic deformation. Each step-in magnification not only deepens our understanding of the fracture characteristics but also corroborates the typical ductile fracture behavior of aluminum alloys.

The initiation of fatigue failure is often identified at a point near the edge of the specimen, where microcracks form as notches along the surface. These cracks typically originate from morphological defects, surface roughness, or irregularities such as micro-voids and microcracks. Once initiated, fatigue failure progresses as the crack expands, leading to material weakening and eventual fracture.

Current understanding highlights the significant role of microstructure in fatigue crack initiation in both pure metals and structural alloys. Key microstructural factors influencing this process include slip bands, grain boundaries, pores, inclusions, and machined surfaces. These elements are critical in explaining the transition from surface-initiated cracks to those originating internally, as well as the occurrence of multiple fatigue limits in some alloys and their absence in others.

In multiphase alloys, microstructure-induced internal stresses can alter stress–life relationships, potentially resulting in dual fatigue limits. These stresses arise from plastic interactions between softer and harder grains, creating plastic

constraint stresses that influence fatigue behavior. Despite these insights, the mechanisms driving fatigue initiation and growth at internal sites remain incompletely understood. Predictive methodologies for accurately forecasting such occurrences are still in developmental stages, underscoring the need for further research to refine our understanding of these complex phenomena.

Figure 13 presents an uneven texture and visible voids that signify ductile behavior. This surface, less uniform than those in previous figures, suggests a complex stress distribution during tensile loading. The higher magnification views in Figures 13(c) and (d) reveal dimples and microvoids, verifying the ductile nature of the fracture. These features demonstrate significant plastic deformation, with microvoid coalescence as the primary fracture mechanism. The rough and irregular morphology, coupled with observed dimples, indicates that the standard tool design, lower spindle speed (800 RPM) and higher feed rate (90 mm/min) produced a coarser microstructure. Although still ductile, this coarser structure led to a less uniform stress distribution compared to finer structures seen in samples welded at higher spindle speeds with a new tool design. This variation highlights the influence of tool design and operational parameters on the fracture behavior of friction stir welded (FSW) joints.

Both samples S1 and S2 display ductile fracture characteristics, marked by dimples and microvoids across various magnifications, indicating significant plastic deformation. However, differences in operational parameters affect their microstructural characteristics. S1, processed with a new tool design at higher spindle speeds (1600 RPM) and lower feed rates (30 mm/min), exhibits a finer microstructure

that enhances ductility. In contrast, S2, prepared with a standard tool design at lower spindle speeds (800 RPM) and higher feed rates (90 mm/min), exhibits a coarser microstructure, leading to a less uniform stress distribution. This comparison emphasizes the significant impact of tool design and operational settings on the fracture behavior and microstructural outcomes in FSW joints.
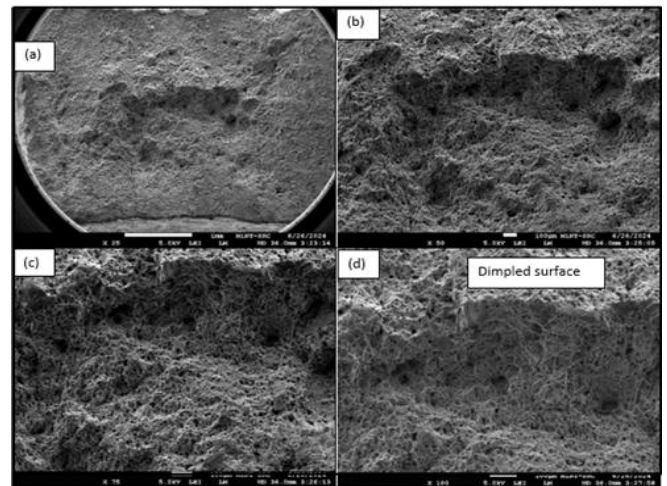
Figure 12. SEM micrographs morphologies showing the fracture surface of sample S1: (a) Overview of the fracture surface displaying the overall morphology and roughness x25; (b) The texture of the fracture surface with visible micro voids, x50; (c) Conical equiaxed dimples observed, x75; (d) Shallow and small dimples indicative of ductile fracture x100
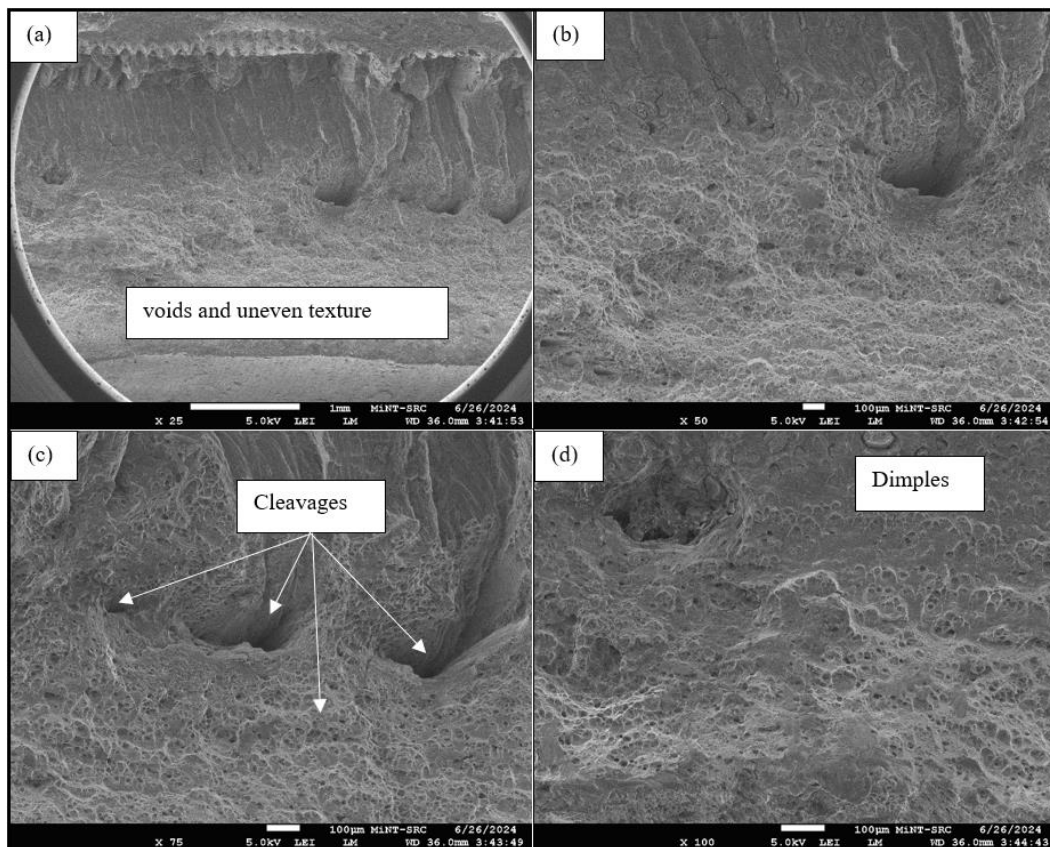
Figure 13. SEM micrographs of sample S2 fatigue test fracture surface at various magnifications: (a) Overview of the fracture surface showing the general topography and the presence of large deformation features, x25; (b) Closer view highlighting finer details of the fracture surface, x50); (c) Presence of microvoids and ductile fracture features, x75); (d) Fine and small dimples, x100

The fracture surface of the welded specimen subjected to fatigue testing was analyzed using a scanning electron microscope (SEM). Observations revealed that the fatigue properties, derived from the S-N curves of welded samples fixed at varying distances from the welding line during testing, closely approached those of the base alloy. SEM fractography of the fracture surface indicated that the primary cause of fatigue failure in the welded samples was the presence of main microcracks, along with secondary and transverse cracks.

The failure predominantly occurred at the weakest points, likely caused by abrupt changes in force equilibrium in the reduced section of the samples welded with the new tool design. The fractographic analysis, shown in Figure 13, highlighted the presence of cleavage fractures and irregular dimples, suggesting a mixed fracture mechanism involving microvoids and cleavage planes. These findings indicate that the innovative tool design significantly influenced the fracture surface characteristics.

The morphology of dimples on fracture surfaces, hypothesized to be influenced by the magnitude of induced stress [22] varies notably across different parameters and tool designs. The presence of both shallow and deep dimples supports this hypothesis, indicating that higher spindle speeds (1600 RPM) and a new tool design can significantly enhance heat input, thereby improving material flow and grain refinement [23]. These changes contribute to increased ductility in the FSW joints, as evidenced in S2. The size and depth of the dimples, indicative of ductility, are primarily determined by the degree of atomic bonding at the coalesced interfaces [24].

The analysis of the fatigue fracture surface of the AA5083-H111/AA6061-T6 joint sample reveals the impact of FSW parameters and tool design on failure mechanisms. Microstructural features in the weld zone, such as fatigue striations, dimples, and secondary cracks, illustrate a mix of ductile and brittle fracture modes. Understanding these characteristics is crucial for optimizing the FSW process and improving the fatigue performance of welded joints in AA5083/AA6061 aluminum alloys. This analysis aids in developing more effective and reliable welding techniques for structural applications.

3.6 Fatigue life modeling for FSW with standard and innovative tool designs

The relationship between stress amplitude (σr) and the number of cycles to failure (N) was modelled using the Basquin equation, derived through a curve-fitting process. The resulting model, depicted in Figure 14, achieved a high coefficient of determination (R^2=0.8925), demonstrating excellent agreement between the predicted and experimental data. This strong correlation highlights the model's ability to accurately capture the fatigue behaviour of the friction stir welded (FSW) samples.

For FSW of AA6061 and AA5083 alloys using the standard tool design, the Basquin equation constants were determined as:

$$A=1011.6 \text{ and } b=-0.116$$

The fatigue life model is expressed as:

$$\sigma r = 1011.6 \cdot N^{-0.116}$$

where,

σr= Stress amplitude
N= Number of cycles to failure
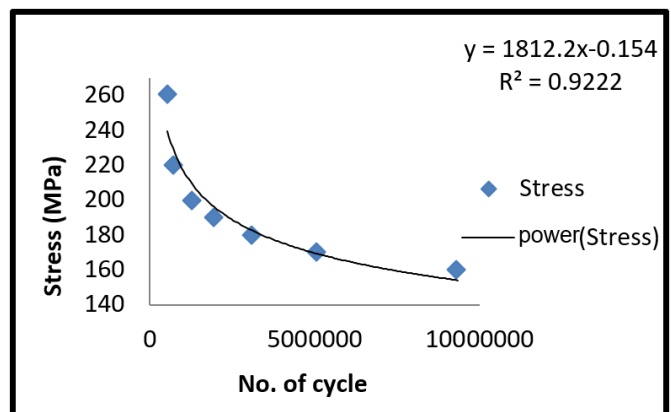A=1011.6 (Material constant (intercept))
b=−0.116 (Fatigue strength exponent).

This formulation effectively captures the influence of stress amplitude on fatigue life for FSW samples welded with the standard tool design. By aligning closely with experimental observations, the model provides a reliable and practical tool for predicting the fatigue performance of these welded materials.
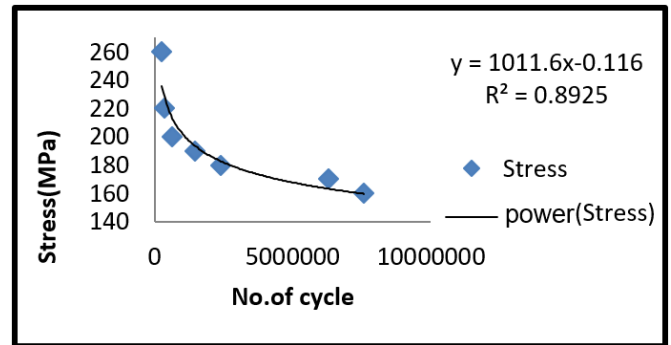
Figure 14. Fatigue behavior of FSW (AA6061 with AA5083) used standard design tool

Figure 15 shows the relationship between stress amplitude (σr) and the number of cycles to failure (N) for friction stir welding (FSW) using the new tool design was modelled using the Basquin equation through a curve-fitting process. This model achieved a coefficient of determination (R^2=0.9222), demonstrating a strong correlation and excellent agreement with the experimental data. This high R^2 value confirms that the predicted values closely match the observed results.

Figure 15. Fatigue behavior of FSW (AA6061 with AA5083) used innovative design tool

For FSW of AA6061 and AA5083 alloys using the new tool design, the Basquin equation constants were determined as:

$$A=1812.2 \text{ and } b=-0.154$$

The fatigue life model is thus expressed as:

$$\sigma r = 1812.2 \ (N)^{-0.154}$$

where,
σr= Stress amplitude

N= Number of cycles to failure
A=1812.2 (Material constant (intercept))
b=−0.154 (Fatigue strength exponent).

This formulation effectively captures the relationship between stress amplitude and fatigue life for FSW samples welded with the standard tool design, providing a reliable and accurate predictive model for assessing their fatigue behavior.

The fatigue life models clearly demonstrate the substantial advantages of the innovative tool design. At a stress amplitude of 160 MPa, joints welded with the innovative tool achieved a fatigue life of 9,328,980 cycles before failure, significantly surpassing the 7,589,146 cycles observed with the standard tool under identical conditions. The innovative tool exhibited significantly improved fatigue resistance, achieving a 23% increase in cycle counts under identical stress levels. However, its fabrication cost is approximately 50% higher due to the complexity of its design. In addition, the tool showed slightly higher wear compared to the standard tool after extended use, likely attributable to increased contact friction from its grooved features. This comparison highlights the pivotal influence of tool geometry and design in enhancing fatigue performance. The innovative tool's superior ability to refine the weld microstructure and induce beneficial residual stresses is a key factor driving its improved durability and performance.

4. CONCLUSIONS

The research objectives were successfully achieved by using a new tool design in friction stir welding (FSW) of dissimilar aluminum alloys (AA5083-H111 and AA6061-T6). Fatigue testing began with constructing an S-N curve, where the material welded with the new tool design endured 9,328,980 cycles at 160 MPa before failure, outperforming the standard tool, which lasted 7,589,146 cycles under the same stress. This increased durability can be attributed to the heat generated during welding, which improves both mechanical and metallurgical properties and induces residual stresses and plastic strains, thus enhancing fatigue strength. Further, a comparative analysis of fracture behavior under fatigue testing revealed that the new tool design led to a more refined microstructure. This is in contrast to the coarser microstructure produced by the standard tool, which operated at a lower spindle speed (800 RPM) and higher feed rate (90 mm/min). The refined microstructure of the new tool design (S1), achieved at higher spindle speeds (1600 RPM) and lower feed rates (30 mm/min), resulted in improved ductility and significant plastic deformation before failure, typical of ductile aluminum alloys where microvoid coalescence is crucial. The tensile strength of the joints made with the new tool design reached 317 MPa, an 18.2% improvement over the 285 MPa achieved with the standard tool. Joint efficiency also increased from 83% to 92.2%. This improvement is likely due to fewer microscopic defects and the recrystallization phenomenon, which promotes the formation of a refined equiaxed grain structure. Microstructural analysis showed that the hardness in the stir zone of joints made with the new tool averaged 122 HV, compared to 101 HV in those made with the standard tool, further highlighting the benefits of the new tool design in FSW.

REFERENCES

[1] Torzewski, J., Grzelak, K., Wachowski, M., Kosturek, R. (2020). Microstructure and low cycle fatigue properties of AA5083 H111 friction stir welded joint. Materials, 13(10): 2381. https://doi.org/10.3390/ma13102381

[2] Li, X., Fang, J., Guan, X. (2021). Unified principal S–N equation for friction stir welding of 5083 and 6061 aluminum alloys. Chinese Journal of Mechanical Engineering, 34: 1-11. https://doi.org/10.1186/s10033-021-00531-0

[3] Ranjan, R., de Oliveira Miranda, A.C., Guo, S.H., Walbridge, S., Gerlich, A. (2019). Fatigue analysis of friction stir welded butt joints under bending and tension load. Engineering Fracture Mechanics, 206: 34-45. https://doi.org/10.1016/j.engfracmech.2018.11.041

[4] Abbass, M.K., Hussein, S.K., Musaa, A.B. (2020). Analysis of fatigue properties in similar friction stir welding joints of aluminum alloy (AA5086-H32). In the Fourth Scientific Conference for Engineering and Postgraduate Research, Baghdad, Iraq. https://doi.org/10.1088/1757-899X/745/1/012059

[5] Mousa, A.B., Abbass, M.K., Hussein, S.K. (2020). Fatigue behavior and fractography in friction stir welding zones of dissimilar aluminum alloys (AA5086-H32 with AA6061-T6). In 3rd International Conference on Sustainable Engineering Techniques (ICSET 2020), Baghdad, Iraq. https://doi.org/10.1088/1757-899X/881/1/012059

[6] Zhang, L., Zhong, H., Li, S., Zhao, H., Chen, J., Qi, L. (2020). Microstructure, mechanical properties and fatigue crack growth behavior of friction stir welded joint of 6061-T6 aluminum alloy. International Journal of Fatigue, 135: 105556. https://doi.org/10.1016/j.ijfatigue.2020.105556

[7] Wang, B.B., Xue, P., Xiao, B.L., Wang, W.G., Liu, Y.D., Ma, Z.Y. (2020). Achieving equal fatigue strength to base material in a friction stir welded 5083-H19 aluminium alloy joint. Science and Technology of Welding and Joining, 25(1): 81-88. https://doi.org/10.1080/13621718.2019.1630571

[8] Mahenran, T., Rajammal, V.K.K.N. (2022). Mechanical and morphological investigation of aluminium 7075 reinforced with nano graphene / aluminium oxide / inconel alloy 625 using ultrasonic stir casting method. Revue des Composites et des Matériaux Avancés-Journal of Composite and Advanced Materials, 32(4): 181-189. https://doi.org/10.18280/rcma.320403

[9] Lu, L., Chen, H., Ren, M., Xu, S., Li, Y., Zhou, T., Yang, Y. (2024). Study on fatigue life of aluminum alloy 6061-T6 based on random defect characteristics. Materials, 17(5): 1133. https://doi.org/10.3390/ma17051133

[10] Chen, Y., Zhang, R.F., He, C., Liu, F.L., Yang, K., Wang, C., Wang, Q.Y., Liu, Y.J. (2020). Effect of texture and banded structure on the crack initiation mechanism of a friction stir welded magnesium alloy joint in very high cycle fatigue regime. International Journal of Fatigue, 136: 105617. https://doi.org/10.1016/j.ijfatigue.2020.105617

[11] Kumar, S., Srivastava, A.K., Singh, R.K., Dwivedi, S.P. (2020). Experimental study on hardness and fatigue behavior in joining of AA5083 and AA6063 by friction stir welding. Materials Today: Proceedings, 25: 646-648. https://doi.org/10.1016/j.matpr.2019.07.535

[12] Salim, B., Imane, B.M., Ahmed, M. (2023). Numerical simulation of asymmetric composite patch repair for fatigue damaged aluminum plate. Revue des Composites et des Matériaux Avancés-Journal of Composite and Advanced Materials, 33(5): 329-338. https://doi.org/10.18280/rcma.330507

[13] Cavaliere, P., Panella, F. (2008). Effect of tool position on the fatigue properties of dissimilar 2024-7075 sheets joined by friction stir welding. Journal of Materials Processing Technology, 206(1-3): 249-255. https://doi.org/10.1016/j.jmatprotec.2007.12.036

[14] Qiao, Y., Zhang, H., Zhao, L., Feng, Q. (2020). Fatigue crack growth properties of AA 5754 aluminum alloy gas tungsten arc welding and friction stir welding joints. Journal of Materials Engineering and Performance, 29: 2113-2124. https://doi.org/10.1007/s11665-020-04739-4

[15] Khalafe, W.H., Sheng, E.L., Bin Isa, M.R., Shamsudin, S.B. (2024). Enhancing mechanical characteristics of 6061-T6 with 5083-H111 aluminum alloy dissimilar weldments: A new pin tool design for friction stir welding (FSW). Metals, 14(5): 534. https://doi.org/10.3390/met14050534

[16] Bakshi, D., Prakash, C., Singh, S., Kumar, R., Ashri, D. (2014). A detailed study on friction stir welding and friction stir processing-A review paper. International Journal of Industrial Engineering & Technology, 4(1): 1-22.

[17] Zainulabdeen, A.A., Abbass, M.K., Ataiwi, A.H., Khanna, S.K., Jashti, B., Widener, C. (2014). Investigation of fatigue behavior and fractography of dissimilar friction stir welded joints of aluminum alloys 7075-T6 and 5052-H34. International Journal of Materials Science and Engineering, 2: 115-121. https://doi.org/10.12720/ijmse.2.2.115-121

[18] Jannet, S., Mathews, P.K., Raja, R. (2014). Comparative investigation of friction stir welding and fusion welding of 6061 T6–5083 O aluminum alloy based on mechanical properties and microstructure. Bulletin of the Polish Academy of Sciences. Technical Sciences, 62(4): 791-795. https://doi.org/10.2478/bpasts-2014-0086

[19] Rajaseelan, S.L., Kumarasamy, S. (2020). Mechanical properties and microstructural characterization of dissimilar friction stir welded AA5083 and AA6061 aluminium alloys. Mechanics, 26(6): 545-552. https://doi.org/10.5755/J01.MECH.26.6.25255

[20] Asmare, A., Al-Sabur, R., Messele, E. (2020). Experimental investigation of friction stir welding on 6061-T6 aluminum alloy using Taguchi-based GRA. Metals, 10(11): 1480. https://doi.org/10.3390/met10111480

[21] Manuel, N., Galvão, I., Leal, R.M., Costa, J.D., Loureiro, A. (2020). Nugget formation and mechanical behaviour of friction stir welds of three dissimilar aluminum alloys. Materials, 13(11): 2664. https://doi.org/10.3390/ma13112664

[22] Li, H., Fu, M.W., Lu, J., Yang, H. (2011). Ductile fracture: Experiments and computations. International Journal of Plasticity, 27(2): 147-180. https://doi.org/10.1016/j.ijplas.2010.04.001

[23] Di Bella, G., Favaloro, F., Borsellino, C. (2023). Effect of process parameters on friction stir welded joints between dissimilar aluminum alloys: A review. Metals, 13(7): 1176. https://doi.org/10.3390/met13071176

[24] Rady, M.H., Mustapa, M.S., Shamsudin, S., Lajis, M.A., Wagiman, A. (2019). Microhardness and microstructure of hot extrusion parameters in direct recycling of aluminium chip (AA 6061) by ANOVA method. In International Conference on Mechanical and Manufacturing Engineering, Johor, Malaysia. https://doi.org/10.1088/1742-6596/1150/1/012069.